Characterization of Infrared Laser systems

Daniel R. Neal*, Darrell J. Armstrong, W. Tim Turner

WaveFront Sciences, Inc.
15100 Central S.E., Albuquerque, NM 87123

Abstract

Laser beam measurement instruments have long been available for visible laser beams, but there is a growing need for such instruments in the near IR. This is especially true for the 1–1.7 μm region that is used for communication lasers. While a few cameras have been developed for this region, there are currently no instruments for measuring laser beam phase that operate in this regime.

We have begun the development of an infrared wavefront sensor based on the Shack-Hartmann principle using an InGaAs IR camera. With this method, the laser beam is dissected into a number of focal spots, which are projected onto a detector. The focal spot position is related to the local wavefront slope. Through appropriate analysis, the laser beam intensity and phase distribution can be obtained.

1. Introduction

In a laser or optical system, the optical quality of the light is the key element that determines the ultimate performance of the system. A beam train is usually constructed from a number of either off-the-shelf or custom components, each of which has a certain set of specifications and errors. With care in the selection of these components, and through careful alignment, it is usually possible to assemble a system that meets expected performance criteria. Often, components are selected that are each better than the final required performance, and through ray-tracing or other modeling. For example, if the final beam must be delivered with λ/4 total RMS wavefront error, then each component may be selected with λ/10 to λ/20 RMS WFE specification. With this method, a system designer can construct a design of an optical system that has a given expected error. With ray-tracing or physical optics modeling, it is possible to even assess alignment errors and tolerances on various components.

The problem, however, is that most of these parameters are known only in the design. Each component may have a different distribution of errors than that specified in the design, or may not actually meet the specifications. Thus the optical system designer is faced with acceptance testing each component of the system. This requires expensive equipment and is time consuming. If strong aspheres are used in the optical design, then testing of individual components may be extremely difficult. In addition, there is no assurance that the final system is aligned well enough that it meets the stated requirements. The only check on the total system is often a beam profile. While some information about the beam quality may be obtained through far-field analysis, this does not provide information about the source of the error, other than general spatial frequency information. In the visible, there are several instruments that have been developed to help with this problem. In some cases, it is even possible to use an interferometer to set up the whole system. But in the IR, few instruments are available, so this problem becomes especially difficult.

One instrument that is beginning to find acceptance for visible optical systems is the Shack-Hartmann wavefront sensor[1]. This instrument relies on extremely simple principles of light: that it travels in a straight line in homogeneous media, and that the wavefront is the surface normal to the local direction of propagation. The sensor operates by dissecting the incoming wavefront into a large number of small subapertures using a lenslet array. This creates a pattern of focal spots on a detector. The position of these focal spots is related to the average wavefront slope across the lenslet subaperture. Thus by measuring the position of these spots, the local wavefront slope can be determined. By integrating these slope measurements spatially, the entire wavefront can be computed. This instrument is thoroughly developed, and it used for a wide variety of applications[2,3,4,5,6,7,8].

* D. R. N. (correspondence): E-mail: drneal@wavefrontsciences.com; www.wavefrontsciences.com; Telephone: (505) 275-4747

Part of the SPIE Conference on Infrared Spaceborne Remote Sensing VI
San Diego, California • July 1998 SPIE Vol. 3437 • 0277-786X/98/$10.00

In order to expand the use of this type of sensor for measuring IR light, we have undertaken the development of an infrared version of the Shack-Hartmann sensor. While previous such instruments have been developed[9], the various technologies have improved significantly in the last several years. Constructing an IR wavefront sensor involves changing many of the components of the visible sensor, while using the same basic concepts. There have been tremendous improvement in the various supporting technologies over the last several years. Both IR camera technology and micro-optics technology have now progressed to the point where a useful IR wavefront sensor is possible. The body of this paper describes the development of a camera system for laser and optics characterization. It should be emphasized that this paper represents a snapshot of the design and development, since the instrument has not been completed at the time of this writing.

1.1 History of Shack-Hartmann sensors

The Shack-Hartmann wavefront sensor was first reported in 1971 as part of NASA and military laser programs[10,11]. The initial sensors were based on discrete lenses and quad cell detectors. These required considerable complexity, since each lens had to be individually mounted and adjusted, and the detectors had a very limited dynamic range. Thus x-y translation was needed for each detector. Aligning and using these detectors was extremely difficult, and they were applied primarily for closed-loop adaptive optics programs. During the late 70s and into the 80s, the fabrication of a lenslet array became possible. These early lenses were made by step-and-repeat processes that resulted in a mold. Multiple lenslet arrays could be made from the same mold. As time progressed, the quality of these elements improved tremendously.

During the late 80s, the technology had improved through the use of CCD cameras[12]. At about this time, the first measurement applications appeared. A Shack-Hartmann sensor was used for measuring the Hubble Space Telescope correction optics[13], and Sandia National Labs developed a number of high speed instruments for turbulence and fluid flow measurements[7, 2]. In the early 90s, binary optics technology was developed that allowed the creation of practical, accurate, and low cost lenslet arrays. Combined with the advances in CCD cameras software, electronics and computers, the modern 2D wavefront sensor became a practical instrument[7, 12]. Today there are still two basic wavefront sensor applications: adaptive optics and measurement. The adaptive optics systems are often one-of-a-kind, customized systems that are used to control a particular deformable mirror[4]. They are optimized for speed, since the adaptive optics system will minimize the need for dynamic range. The use of a SHWFS for measurement is just beginning to gain acceptance for optics and laser testing[1, 8]. The design is somewhat different from that for use with an adaptive optics system, with a larger number of pixels per subaperture needed to provide appropriate dynamic range. These measurement SH sensors have been applied to laser, optics, turbulence and many other applications[1, 2, 8, 14].

1.2 Advantages over other techniques

The key advantage of the Shack-Hartmann wavefront sensor is its simplicity. The sensor head has only two components: a CCD camera and a lenslet array. These may be rigidly attached together to form a robust instrument. Since both the position and brightness distributions of the focal spots may be determined in a single measurement, all of the information may be obtained at once. This is a great advantage over multiple frame interferometry systems (phase-shift interferometry) in vibration tolerance, bandwidth and accuracy. With modern cameras that can be shuttered down to 1/10000 – 1/32000 sec, very little motion will occur during the integration time, even for moderate vibration. This means that these sensors can be used in environments that would otherwise preclude the use of sensitive phase measuring instruments. Applications of these sensors to the industrial shop floor and integration directly into various manufacturing devices is in progress at a number of facilities[8].

In addition to the vibration insensitivity, the SHWFS can have tremendous sensitivity and dynamic range. The sensitivity is determined by the limitations on finding the focal spot positions, while the dynamic range is limited by total focal spot travel. Both of these parameters, with proper design, may be configured for extremely good performance through the use of modern low-noise cameras.

Furthermore, the SHWFS may be used to directly measure a laser beam[1]. While shearing and spatially-filtered interferometers may be used for this purpose, these both have considerable complexity. Furthermore, they may be quite sensitive to alignment errors, making measurements difficult except in extremely stable environments.

2. Shack-Hartmann wavefront sensors

The following section describes the basic method of operation and analysis of a Shack-Hartmann wavefront sensor.

2.1 Method of operation

As shown in Figure 1, the incident aberrated light is dissected by the lenslet array into a number of subapertures. Each of these samples is focused by the lenslet onto the detector. This creates a series of focal spots. The position of each focal spot is proportional to the average tilt over the lenslet sub-aperture. Since the wavefront is defined as the surface that is normal to the direction of propagation, this is also the wavefront slope over each subaperture. Thus reconstruction of the wavefront can be accomplished through integration of the slope distribution.

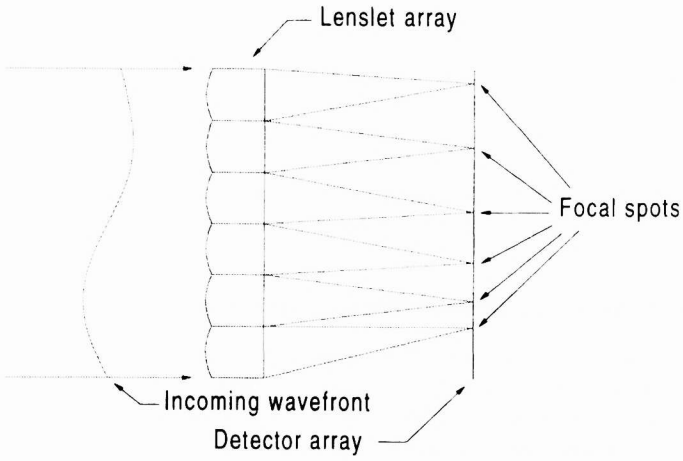

Figure 1 – Basic elements of a Shack-Hartmann wavefront sensor.

The first step is to illuminate the sensor system with the light to be measured, and then acquire data with the camera/lenslet array combination. The images are transferred and stored in a computer for processing.

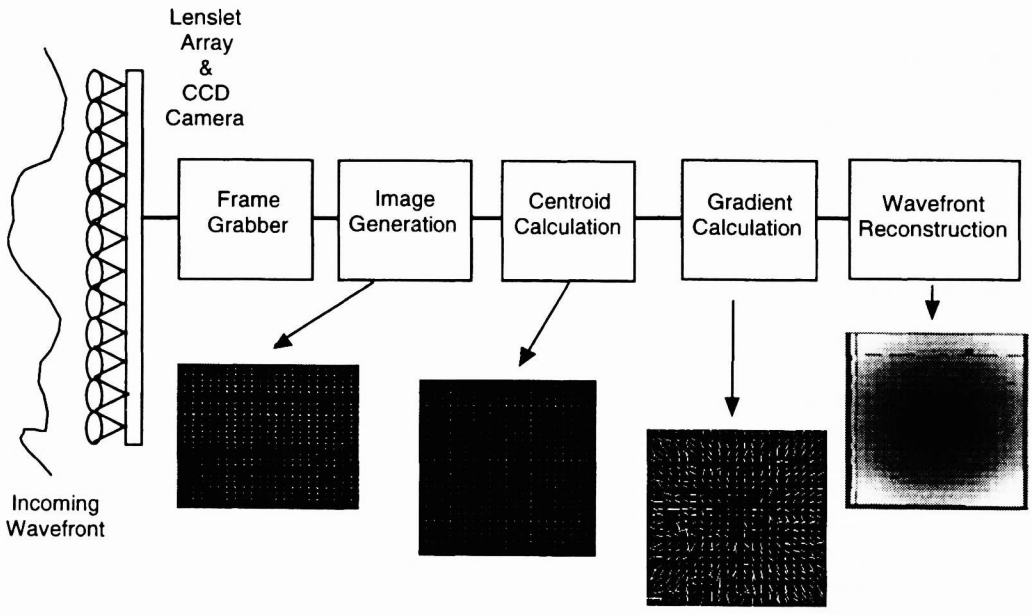

Figure 2 – Basic analysis sequence for Shack-Hartmann wavefront sensor.

2.2 Data analysis

The sequence of operations is described in Figure 2, and outlined below. These data analysis techniques are well established for the visible systems, and operate in exactly the same manner for IR light.

2.2.1 Centroid

The first step in analyzing the data is to determine the positions of the focal spots. For an image $I_{ij,}$ in an area-of-interest $W_{l,\text{ this}}$ can be accomplished using the thresholded centroid algorithm:

$$\hat{\rho}_{l,x} = \frac{\sum_{ij \in W_l} I_{ij} x_{ij}}{\sum_{ij \in W_l} I_{ij}} \tag{0.1}$$

Where the image I_{ij} has been thresholded to eliminate background noise and other effects.

2.2.2 Wavefront slope

The wavefront slopes are computed by comparison to a set of centroids computed from a reference image $\hat{\rho}_{x,REF}$. That is:

$$\theta_{l,x} = \frac{\hat{\rho}_{l,x} - \hat{\rho}_{l,x,REF}}{f_{WFS}} \tag{0.2}$$

2.2.3 Wavefront reconstruction

Once these slopes have been computed, the wavefront error is reconstructed from the gradient equation:

$$\nabla\phi(x,y) = \frac{\partial\phi}{\partial x}\mathbf{i} + \frac{\partial\phi}{\partial y}\mathbf{j} \tag{0.3}$$

This can be accomplished through various means[15]. We have used spline integration and surface fitting with good success[1, 8].

3. IR wavefront sensor design

3.1 System design

The IR wavefront sensor system consists of a number of sub-components. These include beam expander, lenslet array, camera, data acquisition electronics and computer control and processing. A simple set of empirical models have been used to define the performance of the system. These models rely on scaling the measurements from systems with known performance.

3.2 Lenslet array

The lenslet array is the key element needed for making an IR wavefront sensor. Existing visible lenslet arrays cannot be used because the growth in focal spot size due to the longer wavelength will exceed the lenslet dimension. Thus a new lenslet array must be designed and built.

3.2.1 Design

There are a number of ways to design the lenslet array. We have found a useful design rule is to keep the ratio of the lenslet diameter to the focal spot size constant. Existing lenslets with this ratio (N) of N=4 have proven to be very useful for visible systems. To maintain this relationship, the focal length must be chosen such that:

$$f = \frac{d^2}{N\lambda}. \tag{0.4}$$

Thus selecting the lenslet diameter is sufficient to completely specify the lenslet array, given the other parameters. It has also been shown that for even values of the ratio N, the diffractive cross-talk from adjacent lenslets is minimized, at least for near collimated beams[2].

The lenslet diameter is also usually (but not necessarily) chosen to be an integral number of pixels. But the sensitivity (the smallest detectable change in wavefront) and the dynamic range (the largest measurable change) are directly determined by the focal length and lenslet diameter. The design process thus consists of determining the required sensitivity and dynamic range, and the selecting the appropriate number of pixels per lens to give the appropriate combination.

The sensitivity is defined as the minimum detectable change in focal spot position over one lenslet. Thus it is equal to:

$$W_{\min} = \frac{\delta_{\min}}{f} d \tag{0.5}$$

We have found that, in practice, a good rule of thumb for the total peak-to-valley error over the whole aperture can be expressed as:

$$W_{P-V} = \sqrt{N_{samples}} \cdot W_{\min}. \tag{0.6}$$

The nominal definition of dynamic range is where the focal spot just touches the adjacent area-of-interest (AOI). For the lowest order aberration (tilt) this is given by:

$$W_{\max} = \frac{\frac{d}{2} - \frac{f\lambda}{d}}{f} d \cdot N_{samples} \tag{0.7}$$

Parameter	Unit	Design 1	Design 2	Design 3
Camera	Unit	SU 320	SU 320	SU 320
Num lenses X		53	40	32
Num Lenses Y		40	30	24
Lenslet array size X	mm	12.80	12.80	12.80
Lenslet array size Y	mm	9.60	9.60	9.60
Input aperture		14.46	14.46	14.46
Magnification		0.664	0.664	0.664
Lenslet diameter	mm	0.240	0.320	0.400
Focal Length	mm	9.29	16.52	25.81
Dynamic range				
Angular (P-V)	mr	4.29	3.22	2.57
Wavefront per lenslet (P-V)	μm	1.55	1.55	1.55
total wavefront (P-V)	μm	82.67	62.00	49.60
total waves at 1550 nm (P-V)		53.33	40.00	32.00
Sensitivity (noise floor)				
1/100 pixel noise level (RMS)	μr	28.59	16.08	10.29
Total	μm	0.075	0.049	0.035
In Waves		0.049	0.032	0.023
1/λ		21	32	44
Dynamic range factor		1698	1961	2192

Table 1 - Wavefront sensor design parameters

Table 1 shows these values for several possible design choices for the IR sensor system.

3.2.2 Fabrication in IR materials

Once a design has been selected, the lenslet array must be fabricated in the appropriate material. We have made lenslet arrays using micro-optics technology (sometimes called diffractive optics). This technique relies on photolithography and etching for lens array fabrication. There are several different approaches to fabricating these optics. These include multi-level binary optics, half-tone gray scale, and gray-scale mask processes[16]. We typically use the gray scale process because it needs only a single mask, and because of the greater number of potential phase levels.

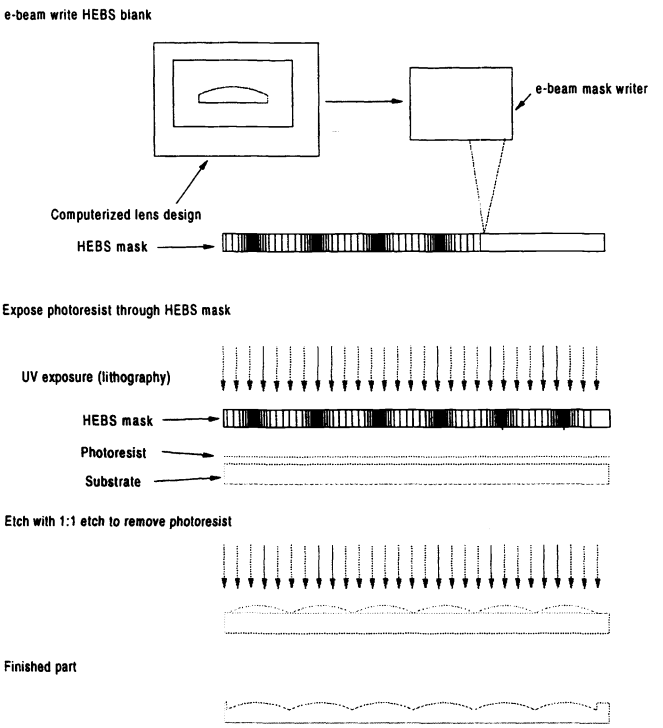

Figure 3-Gray scale micro-optics fabrication process.

For the gray-scale process, the lens surface is described through a design program point by point, and written onto a mask. This mask looks much like a photographic negative, with varying regions of optical density that define the lenslet surface. Photoresist is spun on to the substrate in a thin layer and exposed through the mask. After development, this results in variations in photoresist thickness that corresponds to the exposure. The resist is then etched until the pattern is transferred completely into the substrate.

The key difficulty for an IR detector is the limitation on the total etch depth. In fused silica the index of refraction is fairly low. Thus the total etch depth must be about 3.3 μm. Current etch rates for fused silica and photoresist are in the ratio of 1:0.35 (PR:FS). This means that for AZ 4330, patterned to a total depth of 4.5 μm, the maximum obtainable etch depth in fused silica is ~1.5 μm. Clearly the etch ratio must be improved for use in the IR. Improving this ratio requires selection of a different etch chemistry. Currently, we have used CF_4:O_2 mixtures in a relatively low power rf-field. Increasing the field strength, and changing the chemical ratios will affect the etch ratio. This work is currently underway and is showing promising results.

3.3 IR camera

Another key component of the wavefront sensor is the selection of detector array. There are several different technologies that are used for cameras sensitive to light in these wavelengths. Unfortunately, this is a rapidly growing art, and the combination of small pixel size, low bad pixel count, and large format arrays that we are accustomed to for visible operation is not available.

3.3.1 Camera selection

In order to be useful without an inordinate amount of development, the detector array must be integrated to form a complete camera system. This allows use with common frame-grabber boards and other electronics, and minimizes the rest of the required development. Thus we have restricted the list of possible detectors to those for which this integration has already been performed.

In Table 2, a comparison of several different camera types is presented. There are three main manufacturers that produce cameras that operate in the required wavelength range (1-1.7 μm). These are the Inframetrics, Sensors Unlimited, and Spiricon. The Inframetrics camera is a well integrated, robust system in a small package that is

designed for handheld operation. It includes a built in closed-cycle cryo-cooler, and operates at a wide range of wavelengths. In many ways it is an ideal choice for a wavefront sensor system. However, it suffers from two problems that are difficult to surmount. The first is that the cooler has an inherent vibration spectrum. We measured approximately +/- 20 μr when the camera was rigidly mounted. While this in itself is not a large error, it places a bound on the ultimate performance of the system. The other problem, which is more serious, is that the camera has an internal cold stop. This is an aperture that is actually smaller than the detector size that is a few millimeters in front of the detector inside the dewar. When the camera is used for imaging, this helps minimize background effects. However, it greatly complicates the use of this detector for wavefront sensor use.

Description	Inframetrics InfraCAM	Sensors Unlimited 128	Sensor Unlimited 320	Spiricon
Detector	PtSi	InGaAs	InGaAs	Pyro
Resolution	256X256	128X128	320X240	124X124
Pixel size	30 X 30 μm	60 X 60 μm	40 X 40 μm	100 X 100 μm
Cooler	Stirling engine	Peltier	Peltier	None
Spectral band	1–2.5 μm	0.7–1.7 μm	0.7–1.7 μm	0.4–100 μm
Bandwidth	60 Hz	30 Hz	30 Hz	24, 48 Hz

Table 2- IR Camera specifications

The Spiricon detectors have an enormous wavelength range and good overall performance. However, the large pixel size would lead to extremely course sampling when used for a wavefront sensor. Even a 6 X 6 pixel area per lenslet would lead to a 600 μm resolution. This was judged to be unacceptable for most applications.

The Sensors Unlimited cameras have a combination of relatively small pixel size and large pixel count that make them useful for wavefront sensing. In addition, they have been well integrated into a 12-bit digital camera system. This makes interfacing to the rest of the system much simpler. The noise floor is at the 1–2 bit level. Thus fewer pixels are needed across the focal spot to make accurate centroid measurements. In addition, the detector is easily accessible from the front plate and can be AR coated for the desired wavelength range. All in all, these performance features led to our selection of the Sensors Unlimited 320 camera for this project.

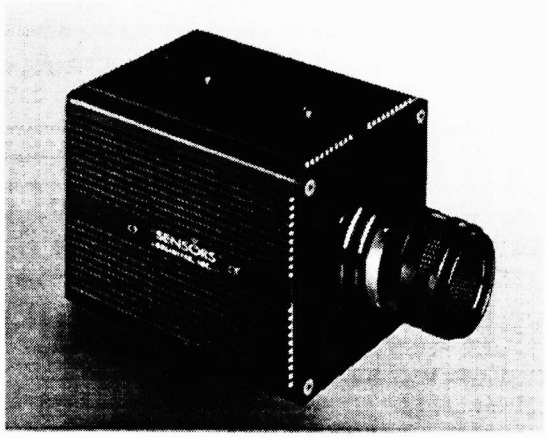

Figure 4 – Sensors Unlimited InGaAs camera with 320X240 resolution

3.3.2 Interface

The Sensors Unlimited 320 camera has a 12-bit digital interface. This was integrated with an Epix PIXCI-D frame grabber for acquisition into the computer. All of the frame grabber functions have been integrated into the CLAS-2D acquisition and analysis code to make operation of the wavefront sensor exactly the same as that for the visible system. In fact, it is possible to put two PIXCI-D cards in the same computer, and hence the same system can be configured for use in both the visible and IR with a simple software switch between operations.

3.3.3 Pixel replacement algorithms

One of the key differences between operation in the visible and IR is the number of dead pixels. It is possible to obtain commercial CCD cameras that operate over the visible range that have 100% good pixels. This is not true for any of the IR cameras. The Sensors Unlimited camera has about 1–2% bad pixels, including clusters and possible column defects. It is possible to select the best sensors from a given manufacturing run, but even these will have many bad pixels.

For imaging, pixel replacement algorithms can be used effectively. However, in a typical wavefront sensor, the spot positions must be determined to 1/10–1/100th of a pixel. Thus the presence of a dead pixel within the area of interest can have a serious effect on the accuracy of estimating the centroid position. Figure 5 shows the effect of a single dead pixel among the central four in an area of interest. The centroid algorithm position is reported as a function of

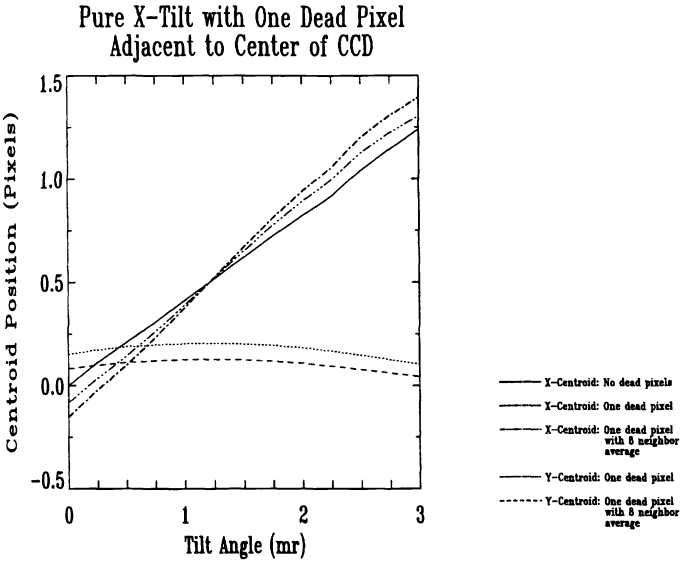

Figure 5 – Effect of dead pixels on centroid algorithm accuracy.

input offset (wavefront slope). With no pixel replacement algorithm, there is a strong (up to ½ pixel) error in this position. This error is reduced by using a nearest neighbor average pixel replacement algorithm, but is not eliminated. It has been shown that cross correlation or matched filter algorithms are much less sensitive to this type of error. Efforts are under way to implement these algorithms and to evaluate their performance.

4. Reference source

Since it is difficult to precisely register the lenslet positions with the detector array pixels, it is often useful to employ a measurement to determine the wavefront reference surface. This has the advantage that other aberrations can be subtracted out of the final measurements, and that this surface is not restricted to a plane wave. In fact, the reference can be any saved data set. Thus the wavefront sensor can be used to compute the difference wavefront from two successive (or otherwise recorded wavefronts). This allows the sensor to be used in complex optical systems to evaluate the effect of one component, or to examine dynamic structures in flow or other fields.

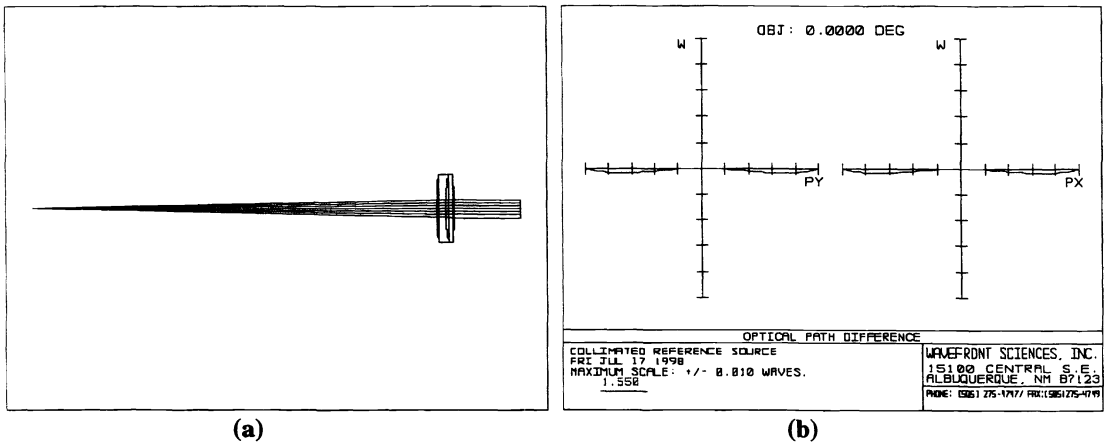

(a) (b)

Figure 6 – Reference source design uses the center part of a high quality achromat to produce a very high quality beam.

In order to use the sensor for absolute measurements, however, a wavefront must be created with known properties. This can be done using the arrangement shown in Figure 6(a). In this arrangement, a single mode fiber is coupled to a laser or other light source, and then collimated using a high quality lens (usually an achromat or asphere). Only a small portion near the center of the lens is sampled by the wavefront sensor. If properly aligned and set up, this results in a beam with an extremely flat (or spherical) wavefront. With a shearing interferometer used to collimate the beam, better than $\lambda/500$ can be achieved over the wavefront sensor aperture, as seen in Figure 6(b).

For our IR sensor, such a source at 1550 was developed. This consisted of a fiber coupled diode laser, and a conventional achromat. Excellent performance is possible using only off-the-shelf lenses.

5. Optomechanical design

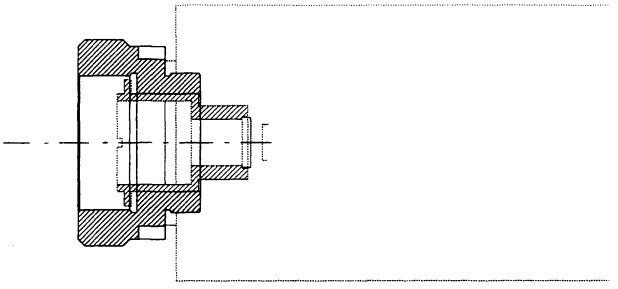

Figure 7 – Optomechanical mounting arrangement for lenslet array to allow rigid mounting to camera.

One key element of our approach is the integration of the lenslet array directly in front of the CCD detector. To this end, the lenslet array must be mounted a fixed distance from the CCD, and a precise method developed for calibrating this distance. In previous work[1], a method was described for determining the offset from a given known position. This method is applied to determine the thickness of a shim that sets the lenslet array to detector distance. In practice we have found that we can determine this position accurately to the nearest $1/1000^{th}$ of an inch.

6. Telescope

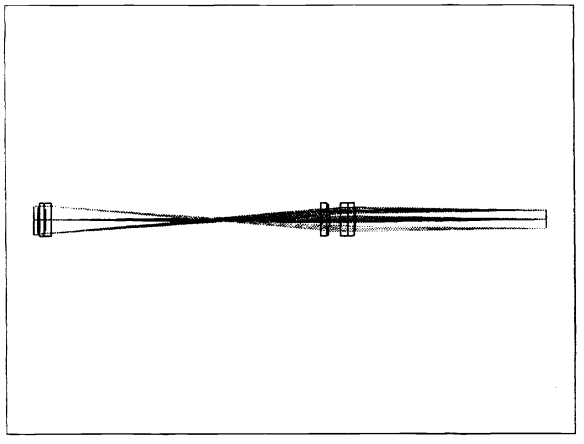

Figure 8 – Telescope for reducing the input beam by Magnification 0.664.

In order to use the wavefront sensor for a number of different sized beams, a telescope is used to reformat the beam to the appropriate size. The optical design of such a telescope is shown in Figure 8. In this figure, the entrance pupil is relay-imaged onto the lenslet array. This design is also completely telecentric, that is, a collimated input produces a collimated output. This is important in that it does not affect the nominal performance of the optical system.

For such a telescope design, operating from object plane to image plane, the ray-matrix transfer function is given by:

$$\begin{bmatrix} M & 0 \\ 0 & 1/M \end{bmatrix} \qquad (0.8)$$

where M is the system magnification (nominally the ratio of the lens focal lengths). For this case it is defined as the ratio of image height to object height. From this matrix, it can be seen that while the linear position of rays (or the size of the image) varies linearly with magnification, the angular magnification is exactly the inverse. This is an important property for a wavefront sensor, since the wavefront sensor does not measure the phase directly, but measures the slope or ray angle. Thus the angle is modified by the input magnification. For systems where this magnification is less than 1, the measured lenslet array focal spot angles will be θ/M. Thus the ray angle is increased. The increased angle will result in greater focal spot motion for a given input angle. The noise level is fixed by camera electronics and other sources. Hence the tilt signal to noise ratio is increased for this case. However, since the sample size is reduced by the magnification, this effect is exactly compensated when the wavefront error is reconstructed. Hence such a telescope has no effect on the wavefront transmitted through the system, other than reducing its spatial extent.

6.1.1 Requirements

To design the appropriate telescope, the appropriate requirements must be specified. As described above, the dual requirements of pupil relay and telecentricity apply. The telescope design consists of selecting the magnification to give the appropriate image size for a given object, and of finding lenses with the appropriate focal lengths. There is one further requirement. The dynamic range of the wavefront sensor is given in Eq.(0.7). However, to avoid vignetting through the optical system, the lenses must be sized to allow collecting light with the appropriate f-number. This is just

$$NA = \frac{d}{4f}. \qquad (0.9)$$

Thus the optical system must include lenses that are capable of collection light with at least this numerical aperture from each point in the pupil.

6.1.2 Optical design

Optical design is aided by an appropriate ray-tracing code. We have used Zemax by Focus Software for most of our calculations. An appropriate telescope design is shown in Figure 8. This design uses off-the-shelf lenses with the appropriate spacing to re-image and demagnify by a factor of 1.5, thus the magnification is 0.667. One feature of this design is that the lenses used will maintain a fixed magnification over a wide wavelength band if the spacing is adjusted. Thus different wavelengths can be used without redesigning the telescope. This telescope has excellent optical performance, and is relatively simple to construct and align.

6.1.3 Optomechanical

The telescope was designed to be mounted in an adjustable tube that could be screwed directly on to the front of the wavefront sensor. The wavefront sensor opto-mechanical elements allow for direct attachment of the telescope.

7. Software and processing considerations

The IR wavefront sensor was designed to be able to directly interface with the software component of WaveFront Sciences' CLAS-2D product. The software is designed for acquisition, analysis and display of data from a Shack-Hartmann sensor. It incorporates all of the algorithms described above, and has a number of different analysis functions. These include centroid, gradient and wavefront false color contour maps, 3D plots of both intensity and wavefront, Zernike decomposition, laser beam M^2, near and far-field propagation and various alignment and set up modes.

Few modifications are needed to apply this software to IR applications. The basic calculations are more or less independent of wavelength. The primary changes that need to be made are due to specific requirements of the camera and data acquisition electronics. Since the CLAS-2D code is capable of recording data from a number of different off-the-shelf frame grabbers, the existing interface code is already in place. The primary code additions are the pixel by pixel gain and offset calculations (flat-fielding), and pixel replacement for missing or dead pixels. These modifications are currently in progress.

8. Conclusions

The paper presents the design of a infrared Shack-Hartmann wavefront sensor for use with 1–1.7 μm light. Since this is a work in progress, we have presented the various design elements, including the optical system, lenslet array, camera, data acquisition and analysis. The design for this sensor has greater than 2000:1 dynamic range, with λ/40 sensitivity.

9. Acknowledgements

The authors would like to acknowledge Sarah Klein of MIT Lincoln Laboratory for her support in this program.

---

[1]D. R. Neal, W. J. Alford, and J. K. Gruetzner, "Amplitude and phase beam characterization using a two-dimensional wavefront sensor," SPIE Vol. **2870**, pp. 72–82 (1996).
[2]D. Neal, R. Pierson, E. Chen, K. Bishop, and L. McMackin, "One dimensional wavefront sensor development for tomographic flow measurements," SPIE vol. **2546**, pp. 378-390 (1995).
[3] D. R. Neal, D. J. Armstrong, E. Hedlund, M. Lederer, A. Collier, C. Spring, J. Gruetzner, G. Hebner and J. Mansell, "Wavefront sensor testing in hypersonic flows using a laser-spark guide star," SPIE Vol. **3172**-36 (1997).
[4] R. Q. Fugate, "Observations of faint objects with laser beacon adaptive optics," SPIE Vol. **2201**, pp. 10–21 (1994).
[5] D. R. Neal, J. D. Mansell, J. K. Gruetzner, R. Morgan, M. E. Warren, "Specialized wavefront sensors for adaptive optics," SPIE Vol. **2534**, pp. 338348 (1995).
[6] L. McMackin , B. Masson, N. Clark, K. Bishop, R. Pierson, and E. Chen, "Hartmann wave front sensor studies of dynamic organized structure in flowfields," AIAA Journal **33** (11), pp. 2158–2164 (Nov. 1995).

[7]D. R. Neal, T. J. O'Hern, J. R. Torczynski, M. E. Warren, and R. Shul, "Wavefront sensors for optical diagnostics in fluid mechanics: application to heated flow, turbulence and droplet evaporation," SPIE Vol. **2005**, pp. 194–203 (1993).
[8] D. R. Neal, D. J. Armstrong, and W. T. Turner, "Wavefront sensors for control and process monitoring in optics manufacture," SPIE **2993**-29 (1997).
[9] C. Higgs, J. W. Bielinski, C. F. Pearson, D. R. Hearn and P. J. Berger, "Infrared Hartmann wavefront sensor,", SPIE **1625**, pp. 365–369 (1992).
[10] R. V. Shack and B. C. Platt, "Production and use of a lenticular Hartmann screen," JOSA **61**(5), p 656 (1971).
[11] L.T. Golden, R. V. Shack, and P. N. Slater, "Study of an instrument for sensing errors in a telescope wavefront," Final Report, Univ. of Arizona, submitted to Marshall Space Flight Center, NASA-CR-120353, May 1974.
[12] D. Kwo, G. Damas and W. Zmek, "A Hartmann-Shack wavefront sensor using a binary optic lenslet array," SPIE **1544**, pp. 66–74 (1991).
[13] T. L. Bruno, A. Wirth, A. J. Jankevics, "Applying Hartmann wavefront sensing technology to precision optical testing of the Hubble Space Telescope correctors," SPIE **1920**, pp. 328–336 (1993).
[14] D. R. Neal, E. Hedlund, M. Lederer, A. Collier, C. Spring, W. Yanta, "Shack-Hartmann wavefront sensor testing of aero-optic phenomena," AIAA **98-2701** (1998).
[15] W. H. Southwell, "Wave-front estimation from wave-front slope measurements," J. Opt. Soc. Am., Vol. **70**, No. 8 (August 1980).
[16] W. Däschner, "Fabrication of diffractive optical elements using a single optical exposure with a gray level mask," J. Vac. Sci. Technol. B, **13**(6) (Nov/Dec 1995).